

Coulomb drag between two graphene layers at different temperatures

F. Escudero ^{1,2,*}, F. Arreyes ¹ and J. S. Ardenghi ^{1,2}

¹*Departamento de Física, Universidad Nacional del Sur, Av. Alem 1253, B8000, Bahía Blanca, Argentina*

²*Instituto de Física del Sur, Conicet, Av. Alem 1253, B8000, Bahía Blanca, Argentina*



(Received 15 September 2022; revised 28 November 2022; accepted 1 December 2022; published 12 December 2022)

We theoretically study the Coulomb drag in graphene when there is a temperature difference between the layers. Within the degenerate limit for equal layer densities, we find that this can lead to significant deviations from the usual quadratic temperature dependence of the drag resistivity. The exact behavior depends strongly on the phase space available for intraband scattering, and is not symmetrical when the temperatures of the layers are interchanged. In particular, when one layer is at a much higher temperature T than the other, the drag resistivity behaves as $\rho_D \sim T/d^5$, where d is the interlayer separation. The magnitude of the drag in this limit is always larger when the active layer is at the higher temperature.

DOI: [10.1103/PhysRevB.106.245414](https://doi.org/10.1103/PhysRevB.106.245414)

I. INTRODUCTION

Many-body interactions play a crucial role in our understanding of many important phenomena in condensed matter physics. Their effect, however, is usually seen indirectly in conventional transport measurements. One important exception is the Coulomb drag effect between two closely spaced layers [1,2], which directly depends on the interlayer many-body interactions. Experimentally, the effect consists of driving a current in one layer and measuring the voltage induced in the other isolated layer. The latter appears due to the interlayer many-body interactions, with the main mechanism being the Coulomb interaction. The quantity of interest is usually the drag resistivity $\rho_D = E_p/j_a$, where E_p is the induced electric field in the passive layer, and j_a is the applied current density in the active layer.

Originally studied in semiconductor heterostructures and quantum wells [3–7], over the last decade there has been considerable interest in the Coulomb drag between two graphene layers [8–14]. As a two-dimensional material, graphene is well known for its relativistic-like dispersion relation at low energies, where electrons behave as chiral massless fermions [15–18]. The ability to easily manipulate the carrier density in graphene leads to unique features in the Coulomb drag. This is particularly reflected at low carrier densities, i.e., close to charge neutrality, where the drag resistivity follows an unconventional dependence with the chemical potential μ and the temperature T [11]. In the degenerate limit $\mu/k_B T \gg 1$, both layers are in the Fermi-liquid regime, and the drag resistivity follows the known quadratic temperature dependence at low temperatures [19–22].

Theoretical calculations of the Coulomb drag usually assume equal temperature layers. This is motivated by conventional experimental measurements in which the temperature varies uniformly throughout the drag setup, including

both layers. Furthermore, due to the required separation between the layers (usually no larger than a few hundred nanometers), it seems impractical, at first sight, to consider a temperature difference between them. However, recent technological advances at the nanoscale may allow one to create (and maintain) a temperature difference between the layers [23–25]. Negligible interlayer heat transfer may be accomplished using low thermal conductivity materials as a dielectric spacer between the layers [26,27].

In the Fermi-liquid regime, the dependence $\rho_D \propto T^2$ is usually understood in terms of phase-space considerations: the momentum transfer between the layers comes from electron-hole excitations, which are limited by the temperature. When the layers are at different temperatures, at first sight one may expect $\rho_D \propto T_a T_p$, where T_a and T_p are the temperatures of the active and passive layer, respectively. However, one should keep in mind that in a typical drag experiment the current is driven through the active layer, where the external electric field is applied. The passive layer is usually isolated, so the drag resistivity only depends on deviations from equilibrium in the distribution function of the active layer. This means that the drag effect should, in principle, depend differently on the temperature of each layer.

In this work, we theoretically investigate the Coulomb drag between two graphene layers at different temperatures. Within the Fermi-liquid regime, we find significant deviations from the usual behavior $\rho_D \propto T^2$. In particular, when the temperature T_i of one layer is much higher than the temperature T_j of the other layer, we find a linear dependence $\rho_D \propto T_i$, practically independent of T_j . The magnitude of the effect depends on the situation: for $T_a \gg T_p$ the drag resistivity is about two times larger than for $T_p \gg T_a$. This reflects the nonsymmetrical behavior of the drag effect when the temperatures of the layers are interchanged. Furthermore, the limit $T_i \gg T_j$ also implies a stronger dependence on the interlayer separation, $\rho_D \propto 1/d^5$, compared to the usual dependence $\rho_D \propto 1/d^4$. We show that these results are strongly related to the allowed intraband transitions in graphene.

*federico.escudero@uns.edu.ar

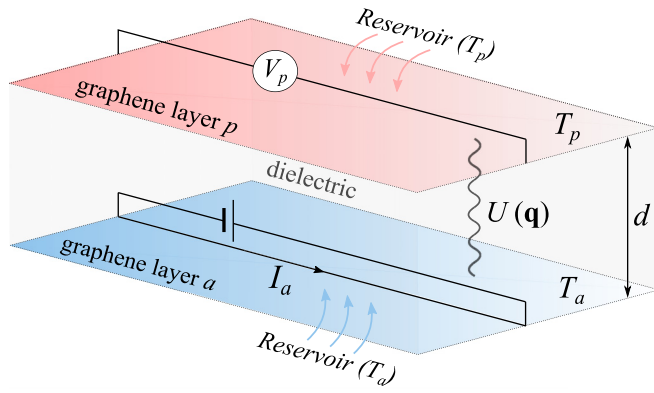


FIG. 1. Schematic configuration of a Coulomb drag setup between two graphene layers. In the active layer a a current I_a is driven, inducing a voltage V_p in the other passive p due to the interlayer Coulomb interaction $U(\mathbf{q})$. The drag resistivity is given by $\rho_D \propto V_p/I_a$. The layers are separated by a distance d by a dielectric medium. Each end is in contact with a different thermal reservoir, which induces a temperature difference $T_a - T_p$ between the graphene layers.

This work is organized as follows: In Sec. II we develop the theoretical model. The drag conductivity is calculated using the kinetic theory approach. The transport is assumed to be dominated by impurities, with a momentum-dependent scattering time. The nonlinear susceptibilities are calculated within the degenerate limit $\mu/k_B T \gg 1$. In Sec. III we present the numerical results for the drag resistivity, as a function of the temperature of each layer. We discuss the drag behavior when the temperature of one layer is fixed, and when there is a fixed temperature difference ΔT between the layers. We also obtain analytical approximations for the drag resistivity in the limit $T_i \gg T_j$. Finally, our conclusions follow in Sec. IV.

II. THEORETICAL MODEL

The system configuration is shown in Fig. 1. Two graphene layers are separated by a distance d , so that no tunneling between them is possible. A current I_a is passed through the active layer ($i = a$), inducing a voltage V_p in the passive layer ($i = p$). Throughout this work, we consider that both layers are electron doped, and in the Fermi-liquid regime $T_F/T \gg 1$. We thus neglect the contribution of plasmons to the drag, which are expected to be relevant at high temperatures $T \gtrsim 0.2T_F$ [28,29], and consider the static screening within the random phase approximation [11]. We assume, for simplicity, equally doped layers and a uniform dielectric spacer with a relative permittivity ϵ_r [21,29,30]. The screened interlayer Coulomb interaction is then given by [31]

$$U_{ap}(\mathbf{q}) = \frac{e^2}{2\epsilon_0\epsilon_r} \frac{q}{(q^2 + 2qq_T)e^{qd} + 2q_T^2 \sinh(qd)}, \quad (1)$$

where $q_T = 4\alpha k_F$ is the Thomas-Fermi wave vector and $\alpha \sim 2.2/\epsilon_r$ is the coupling constant in graphene [15].

Since our interest in this work is to keep the layers at different temperatures, we assume that the dielectric medium is a good thermal insulator [26]. One possibility is to use aerogel as a nanospacer, which has an extremely low thermal

conductivity due to its high porosity and very low density [24,25,27]. This may allow one to keep, during the measurements, the graphene layers at different temperatures if each one is in contact with a thermal reservoir (Fig. 1).

A. Drag conductivity

To obtain the drag conductivity we will use the kinetic theory approach [19,32]. The transport in each layer is assumed to be dominated by impurity scattering, within the ballistic regime. In practice this means that the interlayer separation must be much smaller than the mean free path of the electrons. Consequently, within the relaxation time approximation, to linear order one has [17,32]

$$\tilde{f}_{\mathbf{k},s}^i \simeq f_{\mathbf{k},s}^i + f_{\mathbf{k},s}^i(1 - f_{\mathbf{k},s}^i)\psi_{\mathbf{k},s}^i, \quad (2)$$

where $\psi_{\mathbf{k},s}^i = \beta_i e \mathbf{E}_i \cdot \tau_{\mathbf{k}}^i \mathbf{v}_{\mathbf{k},s}$, with $\beta_i = 1/k_B T_i$. Here $f_{\mathbf{k},s}^i$ and $\tilde{f}_{\mathbf{k},s}^i$ are the equilibrium and nonequilibrium distribution functions in the i layer, $\epsilon_{\mathbf{k},s} = s\hbar v_F k$ is the low energy dispersion relation of electrons in the $s = \pm 1$ band, and $\mathbf{v}_{\mathbf{k},s} = \hbar^{-1} \nabla \epsilon_{\mathbf{k},s}$ is the velocity vector. For charged impurities, the momentum-dependent scattering time reads $\tau_{\mathbf{k}}^i = \tau_i k$ [15,17]. For usual carrier densities in graphene, say $n \sim 10^{12} \text{ cm}^{-2}$, the Fermi-liquid regime holds for temperatures up to $T \sim 100 \text{ K}$.

Following standard manipulations [11,22,28,32], when the layers are at different temperatures the transconductivity is found to be given by

$$\sigma_{ij} = \frac{e^2}{16\pi k_B T_j} \sum_{\mathbf{q}} |U_{ap}(\mathbf{q})|^2 \times \int_{-\infty}^{\infty} d\omega \frac{f_{ij}^{\alpha}(\mathbf{q}, \omega, \Delta\beta)}{\sinh(\beta_i \hbar \omega / 2) \sinh(\beta_j \hbar \omega / 2)}, \quad (3)$$

where α is the current direction, and

$$f_{ij}^{\alpha}(\mathbf{q}, \omega, \Delta\beta) = \Gamma_i^{\alpha}(\mathbf{q}, \omega) [e^{\Delta\beta \hbar \omega / 2} \Gamma_j^{\alpha}(\mathbf{q}, \omega) - 2 \sinh(\Delta\beta \hbar \omega / 2) \tilde{\Gamma}_j^{\alpha}(\mathbf{q}, \omega)], \quad (4)$$

where $\Delta\beta = \beta_i - \beta_j$. The nonlinear susceptibilities read

$$\Gamma_i(\mathbf{q}, \omega) = -2\pi g \sum_{\mathbf{k},s,s'} (f_{\mathbf{k},s}^i - f_{\mathbf{k}+\mathbf{q},s'}^i) F_{s,s'}(\mathbf{k}, \mathbf{q}) \times (\tau_{\mathbf{k}}^i \mathbf{v}_{\mathbf{k}} - \tau_{\mathbf{k}+\mathbf{q}}^i \mathbf{v}_{\mathbf{k}+\mathbf{q}}) \delta_{\mathbf{q},\omega,\mathbf{k}}, \quad (5)$$

$$\tilde{\Gamma}_i(\mathbf{q}, \omega) = -2\pi g \sum_{\mathbf{k},s,s'} (f_{\mathbf{k},s}^i - f_{\mathbf{k}+\mathbf{q},s'}^i) F_{s,s'}(\mathbf{k}, \mathbf{q}) \times [(1 - f_{\mathbf{k},s}^i) \tau_{\mathbf{k}}^i \mathbf{v}_{\mathbf{k},s} - f_{\mathbf{k}+\mathbf{q},s'}^i \tau_{\mathbf{k}+\mathbf{q}}^i \mathbf{v}_{\mathbf{k}+\mathbf{q},s'}] \delta_{\mathbf{q},\omega,\mathbf{k}}, \quad (6)$$

where for brevity we have used the notation $\delta_{\mathbf{q},\omega,\mathbf{k}} \rightarrow \delta(\hbar\omega + \epsilon_{\mathbf{k},s} - \epsilon_{\mathbf{k}+\mathbf{q},s'})$. The factor $g = 4$ takes into account the spin and valley degeneracy. The function

$$F_{s,s'}(\mathbf{k}, \mathbf{q}) = \frac{1 + ss' \cos(\theta_{\mathbf{k}+\mathbf{q}} - \theta_{\mathbf{k}})}{2}, \quad (7)$$

where $\theta_{\mathbf{k}} = \arctan(k_y/k_x)$ comes from the pseudospinors overlap in graphene [15,17].

Equation (3) is quite general, in the sense that the only approximations made are the starting assumptions. For equal

layer temperatures it reduces to the well-known drag conductivity in graphene [8,9,11]. The function $\Gamma_i(\mathbf{q}, \omega)$ is the usual nonlinear susceptibility. The new function $\tilde{\Gamma}_i(\mathbf{q}, \omega)$ only appears in the transconductivity when $T_i \neq T_j$, and as we shall see, it can lead to significant deviations from the drag behavior at equal layer temperatures.

The obtained expression for the transconductivity reflects the two general ways by which the drag depends on the temperature of the layers [2]. One comes from the available electronic states for scattering, which results in the known factor $\sim \sinh^{-1}(\beta\hbar\omega/2)$ (one for each layer). The other temperature dependence comes from the deviations from equilibrium in the distribution function [cf. Eq. (2)]. At equal layer temperatures this simply yields a prefactor $\sim 1/T_j$ in the transconductivity σ_{ij} , and the usual nonlinear susceptibility (5) in both layers (which is temperature independent in the degenerate limit). When $T_i \neq T_j$, the response of the system is modified according to Eq. (4). This function reflects the fact that for interlayer scattering between two layers at different temperatures, the number of states available for scattering into differs from the number of states available for scattering out, even at equilibrium [see Appendix A, Eq. (A3)]. Importantly, the function $f_{ij}^\alpha(\mathbf{q}, \omega, \Delta\beta \neq 0)$ depends on T , even within the degenerate limit $\mu/k_B T \gg 1$.

The drag conductivity (3) is not symmetrical when the temperatures of the layers are interchanged. This behavior is expected due to the configuration of the layers in the drag setup: in the active layer a current is driven, whereas the passive layer is isolated. Consequently, the nonequilibrium response is different in each layer. This also implies that the 2×2 conductivity matrix is not symmetrical when $T_a \neq T_p$, i.e., $\sigma_{ap} \neq \sigma_{pa}$. Note that the asymmetrical behavior of the transconductivity when the layers are interchanged violates the Onsager relation because the two layers are not in thermal equilibrium.

B. Nonlinear susceptibilities

In the Fermi-liquid regime the dominant scattering of electrons is intraband, which allows us to simplify the calculation of the nonlinear susceptibilities by considering only the conduction band. Since $f_{ij}^\alpha(\mathbf{q}, \omega, \Delta\beta) = f_{ij}^\alpha(-\mathbf{q}, -\omega, \Delta\beta)$, it is sufficient to do the calculations for $\omega > 0$. In the limit $\mu/k_B T \gg 1$, at low energies and momenta we have [11,19]

$$\Gamma_i(\mathbf{q}, \omega) \simeq \theta(v_F q - \omega) \frac{g\tau_{\mathbf{k}_F}^i \omega \mathbf{q}}{\pi \hbar v_F q}, \quad (8)$$

where θ is the step function. To evaluate the other function $\tilde{\Gamma}_i$ analytically, we note that in the limit $\mu/k_B T \gg 1$ we have $(-\partial f_{\mathbf{k}}/\partial k) \rightarrow \delta(k - k_F)$. Thus we can take

$$(f_{\mathbf{k}} - f_{\mathbf{k}+\mathbf{q}})f_{\mathbf{k}+\mathbf{q}} \sim \frac{k_F}{\beta\mu} f_{\mathbf{k}} (1 - e^{-\beta\hbar\omega}) \delta_{k, k_F}, \quad (9)$$

$$(f_{\mathbf{k}} - f_{\mathbf{k}+\mathbf{q}})(f_{\mathbf{k}} + f_{\mathbf{k}+\mathbf{q}} - 1) \sim \frac{k_F}{\beta\mu} (\delta_{|\mathbf{k}+\mathbf{q}|, k_F} - \delta_{k, k_F}), \quad (10)$$

where we have used that, by conservation of energy, $|\mathbf{k} + \mathbf{q}| = k + \omega/v_F$. Then the evaluation of $\tilde{\Gamma}_i$ is straightforward; at low

energies and momenta we obtain (cf. Appendix B)

$$\tilde{\Gamma}_i(\mathbf{q}, \omega) \simeq \theta(v_F q - \omega) \frac{g\tau_{\mathbf{k}_F}^i \omega \mathbf{q}}{\pi \hbar v_F q} \frac{1}{\beta_i \hbar \omega} \times \left[\tanh\left(\frac{\beta_i \hbar \omega}{2}\right) - 2\left(\frac{\omega}{v_F q}\right)^2 \right]. \quad (11)$$

C. Drag resistivity

We now focus on the drag resistivity ρ_D , which is what experiments usually measure. Inverting the 2×2 conductivity matrix yields

$$\rho_D = \frac{\sigma_{pa}}{\sigma_{ap}\sigma_{pa} - \sigma_{aa}\sigma_{pp}} \simeq -\frac{\sigma_{pa}}{\sigma_{aa}\sigma_{pp}}, \quad (12)$$

where $\sigma_{ii} = e^2 2\pi v_F \tau_i n_i / h$ is the single layer conductivity in graphene [15] (assuming charged impurities). The last approximation follows from $\sigma_{ij} \ll \sigma_{ii}$, which implies that in the active layer the drag effects are negligible, i.e., $j_a \simeq \sigma_{aa} E_a$. Note that the drag resistivity depends on the transconductivity σ_{pa} (rather than σ_{ap}) [cf. Eq. (3)].

Introducing adimensional variables $x = dq$ and $y = \hbar\omega\beta_a$, the drag resistivity can be written as

$$\rho_D = -\frac{h}{e^2} \frac{g^2}{256\pi} \frac{k_B T_a}{\mu} \frac{k_B T_p}{\mu} \frac{1}{(dq_T)^2} \frac{1}{(dk_F)^2} \times \int dx \frac{x^3 e^{-2x}}{[(x\kappa + 1)^2 - e^{-2x}]^2} G(x, \lambda, \gamma), \quad (13)$$

where $\kappa = 1/dq_T$, and

$$G(x, \lambda, \gamma) = \int_0^{x/\lambda} dy \frac{y\gamma}{\sinh(y/2) \sinh(y\gamma/2)} \left\{ y e^{-y(1-\gamma)/2} + 2 \sinh\left[\frac{y}{2}(1-\gamma)\right] \left[\tanh\left(\frac{y}{2}\right) - 2\left(\lambda \frac{y}{x}\right)^2 \right] \right\}. \quad (14)$$

Here $\lambda = dk_B T_a / \hbar v_F$ and $\gamma = T_a / T_p$. The upper limit x/λ in the integration over y comes from the allowed intraband transitions ($\omega < v_F q$) [15], which leads to a linear dependence $\rho_D \propto T$ for equal temperature layers and large values of λ (i.e., high temperatures and large interlayer separations) [22,33,34].

Clearly, for arbitrary T_a and T_p the temperature dependence of the drag resistivity (13) does not follow a simple power law. The usual Fermi-liquid result $\rho_D \propto T^2$ is obtained only when $\gamma = 1$ and $\lambda \ll 1$, which implies $G \simeq 4\pi^2/3$ [22]. Note that the prefactor $\sim 1/\mu^2$ in Eq. (13) (for doped layers with equal carrier density; in general $\sim 1/(\mu_a \mu_p)$) implies that the drag always requires electron-hole asymmetry [2]. This behavior is expected for the leading order drag effect [35,36], which is equivalent to the kinetic theory approach used to obtain the transconductivity [11]. In particular, in the strong screening limit $\kappa \ll 1$ the drag resistivity in the Fermi-liquid regime depends on the carrier density as $\rho_D \propto 1/(n_a n_p)^{3/2}$ [8], regardless of the temperature difference between the layers.

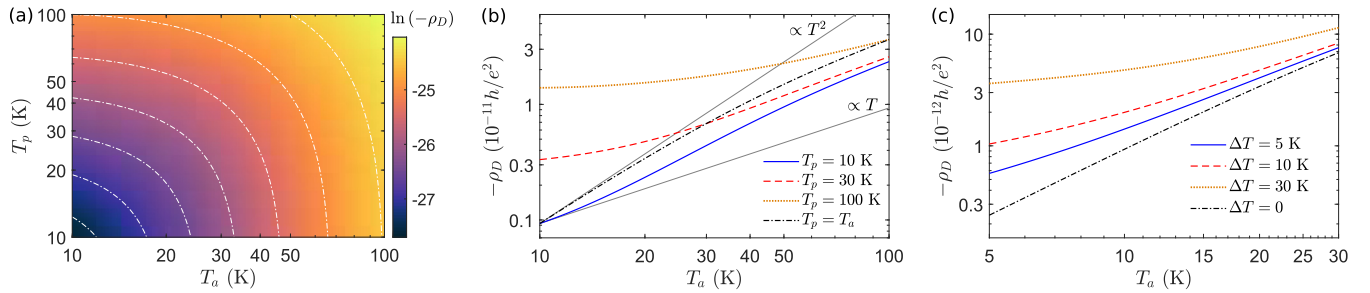


FIG. 2. (a) Density plot of the drag resistivity ρ_D in logarithmic scale (in units of h/e^2), as a function of the temperatures T_a and T_p of the active and passive layers, respectively. The white dot-dashed lines correspond to constant values of $\ln(-\rho_D)$, in steps of 0.5. (b) Drag resistivity as a function of T_a , for fixed values of T_p . Solid black lines represent $\rho_D \propto T^2$ and $\rho_D \propto T$ behavior. (c) Drag resistivity as a function of T_a , for fixed temperature differences $\Delta T = T_p - T_a$. In the last two figures, the black dot-dashed line is the drag resistivity at equal temperatures. In all cases we consider an interlayer separation $d = 100$ nm, carrier density $n = 10^{12}$ cm $^{-2}$, and coupling constant $\alpha = 2$.

III. RESULTS AND DISCUSSION

In general, the integration of Eq. (13) can only be done numerically. We will consider relatively large interlayer separations ($dk_F \gg 1$), so that any heat transfer between the layers is kept at a minimum. For typical carrier densities $n \sim 10^{12}$ cm $^{-2}$, the condition $dk_F \gg 1$ is satisfied for $d \gtrsim 50$ nm. Furthermore, since the dielectric constant of aerogel materials is very low [37,38], we consider a coupling constant $\alpha \sim 2$ in graphene, close to its vacuum value ~ 2.2 [15]. We note, however, that many-body effects within each graphene layer may renormalize α towards lower values [39,40].

A. Numerical results

The numerical results for the drag resistivity are shown in Fig. 2. The density plot in Fig. 2(a) illustrates that the drag depends significantly on the temperature difference between the graphene layers. It also clearly shows that the drag behavior is not symmetrical when the layer temperatures are interchanged. In particular, when $T_a \gg T_p$ the drag resistivity is larger than when $T_a \ll T_p$.

When the temperature T_j of one layer is kept fixed as the temperature T_i of the other layer is varied, the drag resistivity as a function of T_i clearly deviates from the usual quadratic temperature dependence $\rho_D \propto T_i^2$ [Fig. 2(b)]. The effect is more pronounced when $T_i \ll T_j$, which implies low temperatures T_i . This behavior should be contrasted with the known crossover to a linear dependence $\rho_D \propto T$ in the usual case $T_a = T_p$, which only occurs at relatively high temperatures [22,33,34]. Note that Fig. 2(b) is not symmetrical under a temperature exchange, in the sense that varying T_p while keeping T_a constant yields a different drag resistivity magnitude.

Figure 2(c) shows the drag resistivity when both T_a and T_p vary, but in such a way that there is always a constant temperature difference $\Delta T = T_p - T_a$. This situation may represent temperature fluctuations in a conventional experiment, where the ideal situation $T_a = T_p$ may not be exactly realized. The resulting deviations from $\rho_D \propto T^2$ can still be quite significant, even at relatively small temperature differences between the layers. In general, considering ρ_D as a function of T_a , the deviations from the dependence $\rho_D \propto T_a^2$ are more pronounced when $|\Delta T|$ is comparable to (or larger than) T_a , which, in practical terms, implies low temperatures T_a .

Significant deviations from the behavior $\rho_D \propto T^2$ in the Fermi-liquid regime are usually attributed to the appearance of other drag mechanisms, such as the frictional drag mediated by phonon-electron interactions [41–43]. In contrast, the deviations from the T^2 behavior shown in Fig. 2 arise only from the effect of a temperature difference between the layers on the drag relaxation rate. In graphene, the phonon-mediated drag becomes important only at relatively high temperatures $T \gtrsim 150$ K [42]. For the Coulomb drag at equal layer temperatures, the deviation to a linear dependence $\rho_D \propto T$ begins to take place at roughly $\lambda = dk_B T / \hbar v_F \sim 0.2$ [22], although it becomes significant only for $\lambda \gtrsim 1$, which for $d = 100$ nm implies $T \gtrsim 75$ K [see Fig. 2(b)]. Consequently, within the Fermi-liquid regime, significant deviations from the T^2 behavior at low temperatures can only occur when the graphene layers are at different temperatures.

Although we have focused on the Coulomb drag between two graphene monolayers, our results are also relevant for the Coulomb drag between two, two-dimensional electron gases [5,44], two graphene bilayers [14,19,45], or different layered materials [46,47]. Equation (3) is readily generalized to these cases, provided that one uses the corresponding dispersion relation, form factor, and scattering time. Since Eq. (6) is in general temperature dependent (even within the degenerate limit), the quantitative effect of a temperature difference between the layers on the drag resistivity is expected to be system dependent. The universal quadratic temperature behavior $\rho_D \propto T^2$ (i.e., regardless of the electronic properties of the layers) holds only at equal layer temperatures, where the transconductivity only depends on the nonlinear susceptibility (5), which to leading order is temperature independent in the Fermi-liquid regime. In this sense, the Coulomb drag depends more strongly on the electronic properties of the layers if they are at different temperatures.

B. Analytical approximations

The temperature dependence of the drag when $T_a \neq T_p$ can be understood by analyzing the limiting behaviors of the function (14), for the limits $\gamma \ll 1$ and $\gamma \gg 1$. Since we are considering $dk_F \gg 1$ and $\alpha \sim 2$, the factor $\kappa \ll 1$ in Eq. (13) will be ignored [22,34].

In the Fermi-liquid regime, where $k_B T_a / \mu \ll 1$, the case $\gamma \ll 1$ necessarily implies low temperatures in the active

layer, so that $\lambda \ll 1$ (technically, if dk_F is very large, one may have $\lambda \sim 1$ even if $k_B T_a / \mu$ is very small; however, this implies very large interlayer separations and carrier densities, a special situation which we shall neglect). Similarly, the opposite case $\gamma \gg 1$ implies high values of λ . Thus for $\gamma \ll 1$ the integrand in Eq. (14) can be expanded to lowest order in γ , whereas for $\gamma \gg 1$ the integrand can be expanded to lowest order in y . [The latter approximation holds because the x integral in Eq. (13) implies a cutoff at low values of x .] We then have, to leading order in x ,

$$G(x, \lambda, \gamma) \simeq \frac{4x}{3\lambda} \begin{cases} 1, & \gamma \ll 1 \\ 2\gamma, & \gamma \gg 1. \end{cases} \quad (15)$$

Replacing in Eq. (13) yields

$$\rho_D \simeq -\frac{\hbar \pi^3}{e^2} \frac{k_B / \mu}{720 (dq_T)^2 (dk_F)^3} \begin{cases} T_p / 2, & \gamma \ll 1 \\ T_a, & \gamma \gg 1. \end{cases} \quad (16)$$

Thus, when $T_i \gg T_j$, the phase space available for electron-hole pairs is limited by the higher temperature T_i . Both limits of γ also imply a stronger dependence on the interlayer separation, $\rho_D \propto 1/d^5$, which is the same behavior obtained when $T_a = T_p$, at large temperatures. Note that the drag resistivity in the limit $T_a \gg T_p$ is twice as large as in the opposite limit [see Fig. 2(a)].

IV. CONCLUSIONS

We have theoretically studied the Coulomb drag between two graphene layers at different temperatures. Our analysis holds for doped graphene layers with equal carrier density, within the degenerate limit $\mu / k_B T \gg 1$ and in the ballistic regime. In terms of the temperatures T_a and T_p of the active and passive layers, respectively, we have found significant deviations from the usual quadratic temperature dependence in the drag resistivity when $T_a \neq T_p$. In particular, in the limit $T_i \gg T_j$ the drag resistivity depends only on the much higher temperature as $\rho_D \propto T_i$. The magnitude of this behavior is not symmetrical: when $T_a \gg T_p$ the drag resistivity is about twice as large as in the opposite case. This behavior holds in general, in the sense that ρ_D is not symmetrical when the temperatures of the layers are interchanged. Furthermore, the limit $T_i \gg T_j$ also implies a stronger dependence $\rho_D \propto 1/d^5$ on the interlayer separation d . The obtained results can be pronounced even at relatively small temperature differences between the layers. Thus, experimental deviations from the usual behavior $\rho_D \propto T^2$ may be attributed to thermal fluctuations.

ACKNOWLEDGMENTS

This paper was partially supported by grants of CONICET (Argentina National Research Council) and Universidad Nacional del Sur (UNS) and by ANPCyT through PICT 2019-03491 Res. No. 015/2021, and PIP-CONICET 2021-2023 Grant No. 11220200100941CO. J.S.A. acknowledges support as a member of CONICET, F.E. acknowledges support from a research fellowship from this institution, and F.A. acknowledges support as a member of Departamento de Física, Universidad Nacional del Sur.

APPENDIX A: TRANSCONDUCTIVITY BETWEEN TWO GRAPHENE LAYERS AT DIFFERENT TEMPERATURES

The current can be separated by its contributions from intraband impurity scattering and interlayer scattering [19], $\mathbf{j}_i = \mathbf{j}_i^{\text{imp}} + \mathbf{j}_i^{\text{inter}}$, where $\mathbf{j}_i^{\text{imp}} = \sigma_{ii} \mathbf{E}_i$ and $\mathbf{j}_i^{\text{inter}} = ge \sum_{\mathbf{k}, s} \mathbf{v}_{\mathbf{k}, s} \tau_{\mathbf{k}}^i \mathcal{I}_{\mathbf{k}, s}^{i, \text{inter}}$. Here $\mathcal{I}_{\mathbf{k}, s}^{i, \text{inter}}$ is the collision integral due to the interlayer interaction:

$$\begin{aligned} \mathcal{I}_{\mathbf{k}, s}^{i, \text{inter}} = & \sum_{\mathbf{k}', \mathbf{q}} \sum_{s', r, r'} \mathcal{W}_{s, s', r, r'}(\mathbf{k}, \mathbf{k}', \mathbf{q}) [\tilde{f}_{\mathbf{k}+\mathbf{q}, s'}^i \tilde{f}_{\mathbf{k}'-\mathbf{q}, r'}^j (1 - \tilde{f}_{\mathbf{k}, s}^i) (1 - \tilde{f}_{\mathbf{k}', r}^j) \\ & - \tilde{f}_{\mathbf{k}, s}^i \tilde{f}_{\mathbf{k}', r}^j (1 - \tilde{f}_{\mathbf{k}+\mathbf{q}, s'}^i) (1 - \tilde{f}_{\mathbf{k}'-\mathbf{q}, r'}^j)] \delta(\epsilon_{\mathbf{k}, s} + \epsilon_{\mathbf{k}', r} - \epsilon_{\mathbf{k}+\mathbf{q}, s'} - \epsilon_{\mathbf{k}'-\mathbf{q}, r'}), \end{aligned} \quad (A1)$$

where $\mathcal{W}_{s, s', r, r'}(\mathbf{k}, \mathbf{k}', \mathbf{q})$ is the interlayer scattering probability for $|\mathbf{k}, s; \mathbf{k}', r\rangle \rightarrow |\mathbf{k} + \mathbf{q}, s'; \mathbf{k}' - \mathbf{q}, r'\rangle$. Within Fermi's golden rule,

$$\mathcal{W}_{s, s', r, r'}(\mathbf{k}, \mathbf{k}', \mathbf{q}) = \frac{2\pi g}{\hbar} |U_{ap}(\mathbf{q})|^2 F_{s, s'}(\mathbf{k}, \mathbf{q}) F_{r, r'}(\mathbf{k}', -\mathbf{q}). \quad (A2)$$

Replacing Eq. (2), using conservation of energy, and the relation

$$f_{\mathbf{k}+\mathbf{q}, s'}^i f_{\mathbf{k}'-\mathbf{q}, r'}^j (1 - f_{\mathbf{k}, s}^i) (1 - f_{\mathbf{k}', r}^j) = f_{\mathbf{k}, s}^i f_{\mathbf{k}', r}^j (1 - f_{\mathbf{k}+\mathbf{q}, s'}^i) (1 - f_{\mathbf{k}'-\mathbf{q}, r'}^j) e^{-\Delta\beta\Delta\epsilon}, \quad (A3)$$

where $\Delta\beta = \beta_i - \beta_j$ and $\Delta\epsilon = \epsilon_{\mathbf{k}+\mathbf{q}, s'} - \epsilon_{\mathbf{k}, s}$, gives $\mathbf{j}_i^{\text{inter}} = \mathbf{j}_{i,0}^{\text{inter}} + \mathbf{j}_{i,1}^{\text{inter}}$, where (to linear order in ψ)

$$\begin{aligned} \mathbf{j}_{i,0}^{\text{inter}} = & -ge \sum_{\mathbf{k}, \mathbf{k}', \mathbf{q}} \sum_{s, s', r, r'} \mathcal{W}_{s, s', r, r'}(\mathbf{k}, \mathbf{k}', \mathbf{q}) \mathbf{v}_{\mathbf{k}, s} \tau_{\mathbf{k}}^i f_{\mathbf{k}, s}^i f_{\mathbf{k}', r}^j (1 - f_{\mathbf{k}+\mathbf{q}, s'}^i) (1 - f_{\mathbf{k}'-\mathbf{q}, r'}^j) \\ & \times (e^{-\Delta\beta\Delta\epsilon} - 1) \delta(\epsilon_{\mathbf{k}, s} + \epsilon_{\mathbf{k}', r} - \epsilon_{\mathbf{k}+\mathbf{q}, s'} - \epsilon_{\mathbf{k}'-\mathbf{q}, r'}), \end{aligned} \quad (A4)$$

$$\begin{aligned}
 \mathbf{j}_{i,1}^{\text{inter}} = & -ge \sum_{\mathbf{k}, \mathbf{q}} \sum_{s, s', r, r'} \mathcal{W}_{s, s', r, r'}(\mathbf{k}, \mathbf{k}', \mathbf{q}) \mathbf{v}_{\mathbf{k}, s} \tau_{\mathbf{k}}^i f_{\mathbf{k}, s}^i f_{\mathbf{k}', r}^j (1 - f_{\mathbf{k}+\mathbf{q}, s'}^i) (1 - f_{\mathbf{k}'-\mathbf{q}, r'}^j) \\
 & \times \left\{ (\psi_{\mathbf{k}, s}^i + \psi_{\mathbf{k}', r}^j - \psi_{\mathbf{k}+\mathbf{q}, s'}^i - \psi_{\mathbf{k}'-\mathbf{q}, r'}^j) + (e^{-\Delta\beta\Delta\epsilon} - 1) [f_{\mathbf{k}, s}^i \psi_{\mathbf{k}, s}^i + f_{\mathbf{k}', r}^j \psi_{\mathbf{k}', r}^j \right. \\
 & \left. - \psi_{\mathbf{k}+\mathbf{q}, s'}^i (1 - f_{\mathbf{k}+\mathbf{q}, s'}^i) - \psi_{\mathbf{k}'-\mathbf{q}, r'}^j (1 - f_{\mathbf{k}'-\mathbf{q}, r'}^j)] \right\} \delta(\epsilon_{\mathbf{k}, s} + \epsilon_{\mathbf{k}', r} - \epsilon_{\mathbf{k}+\mathbf{q}, s'} - \epsilon_{\mathbf{k}'-\mathbf{q}, r'}). \quad (\text{A5})
 \end{aligned}$$

The contribution $\mathbf{j}_{i,0}^{\text{inter}}$, which is independent of the electric fields (does not depend on ψ) and only appears when $\Delta\beta \neq 0$, vanishes when integrated over \mathbf{q} . Then, replacing $\psi_{\mathbf{k}, s}^i = \beta_i e \mathbf{E}_i \cdot \tau_{\mathbf{k}}^i \mathbf{v}_{\mathbf{k}, s}$, using the relations

$$f_{\mathbf{k}, s}^i f_{\mathbf{k}', r}^j (1 - f_{\mathbf{k}+\mathbf{q}, s'}^i) (1 - f_{\mathbf{k}'-\mathbf{q}, r'}^j) = -\frac{e^{\Delta\beta\Delta\epsilon/2} (f_{\mathbf{k}, s}^i - f_{\mathbf{k}+\mathbf{q}, s'}^i) (f_{\mathbf{k}', r}^j - f_{\mathbf{k}'-\mathbf{q}, r'}^j)}{4 \sinh(\beta_i \Delta\epsilon/2) \sinh(\beta_j \Delta\epsilon/2)}, \quad (\text{A6})$$

$$\mathcal{W}_{s, s', r, r'}(\mathbf{k}, \mathbf{k}', \mathbf{q}) = \mathcal{W}_{s', s, r', r}(\mathbf{k} + \mathbf{q}, \mathbf{k}' - \mathbf{q}, -\mathbf{q}), \quad (\text{A7})$$

and standard manipulations [32], yields the transconductivity given in the main text.

APPENDIX B: CALCULATION OF $\tilde{\Gamma}_i(\mathbf{q}, \omega)$

Considering a momentum-dependent scattering time $\tau_{\mathbf{k}}^i = \tau_i k$, and only the conduction band, Eq. (6) reads

$$\begin{aligned}
 \tilde{\Gamma}_i(\mathbf{q}, \omega) = & 2\pi g \tau_i v_F \mathbf{q} \sum_{\mathbf{k}} (f_{\mathbf{k}}^i - f_{\mathbf{k}+\mathbf{q}}^i) f_{\mathbf{k}+\mathbf{q}}^i F(\mathbf{k}, \mathbf{q}) \delta(\hbar\omega + \epsilon_{\mathbf{k}} - \epsilon_{\mathbf{k}+\mathbf{q}}) \\
 & + 2\pi g \tau_i v_F \sum_{\mathbf{k}} \mathbf{k} (f_{\mathbf{k}}^i - f_{\mathbf{k}+\mathbf{q}}^i) (f_{\mathbf{k}}^i + f_{\mathbf{k}+\mathbf{q}}^i - 1) F(\mathbf{k}, \mathbf{q}) \delta(\hbar\omega + \epsilon_{\mathbf{k}} - \epsilon_{\mathbf{k}+\mathbf{q}}). \quad (\text{B1})
 \end{aligned}$$

The calculation will be done for $\omega > 0$. Taking into account the change of angle $\theta = \theta_{\mathbf{k}} - \theta_{\mathbf{q}}$, we have

$$\mathbf{k} \rightarrow \frac{\mathbf{q}}{q} k \cos \theta + \frac{\mathbf{e}_z \times \mathbf{q}}{q} k \sin \theta. \quad (\text{B2})$$

Due to the delta functions, the term proportional to $\sin \theta$ vanishes after the integration over θ . Then, writing

$$F(\mathbf{k}, \mathbf{q}) = \frac{1}{2} \left(1 + \frac{k + q \cos \theta}{|\mathbf{k} + \mathbf{q}|} \right), \quad (\text{B3})$$

the integration of the delta over the angle θ gives

$$\tilde{\Gamma}_i(\mathbf{q}, \omega) = \theta(v_F q - \omega) \frac{g \tau_i v_F}{2\pi \hbar v_F} \frac{\mathbf{q}}{\sqrt{(q^2 - \tilde{\omega}^2)}} [X_i(\mathbf{q}, \omega) + Y_i(\mathbf{q}, \omega)], \quad (\text{B4})$$

where

$$X_i(\mathbf{q}, \omega) = \int_{(q-\tilde{\omega})/2}^{\infty} dk (f_k^i - f_{k+\tilde{\omega}}^i) f_{k+\tilde{\omega}}^i \sqrt{(\tilde{\omega} + 2k)^2 - q^2}, \quad (\text{B5})$$

$$Y_i(\mathbf{q}, \omega) = \int_{(q-\tilde{\omega})/2}^{\infty} dk (f_k^i - f_{k+\tilde{\omega}}^i) (f_k^i + f_{k+\tilde{\omega}}^i - 1) \sqrt{(\tilde{\omega} + 2k)^2 - q^2} \frac{\tilde{\omega}^2 + 2k\tilde{\omega} - q^2}{2q^2}, \quad (\text{B6})$$

with $\tilde{\omega} = \omega/v_F$. Replacing the relations (9) and (10) yields

$$X_i(\mathbf{q}, \omega) = \theta \left(k_{F,i} - \frac{q + \tilde{\omega}}{2} \right) \frac{k_{F,i}}{\beta_i \mu_i} \tanh \left(\frac{\beta_i \hbar \omega}{2} \right) \sqrt{(\tilde{\omega} - 2k_{F,i})^2 - q^2}, \quad (\text{B7})$$

$$Y_i(\mathbf{q}, \omega) = \sum_{\ell=\pm} \theta \left(k_{F,i} - \frac{q + \ell \tilde{\omega}}{2} \right) \ell \frac{k_{F,i}}{\beta_i \mu_i} \sqrt{(\tilde{\omega} - \ell 2k_{F,i})^2 - q^2} \frac{-\ell \tilde{\omega}^2 + 2k_{F,i} \tilde{\omega} - q^2}{2q^2}. \quad (\text{B8})$$

Expanding the above expressions to lowest order in ω and q results in Eq. (11).

[1] A. G. Rojo, *J. Phys.: Condens. Matter* **11**, R31 (1999).

[2] B. N. Narozhny and A. Levchenko, *Rev. Mod. Phys.* **88**, 025003 (2016).

[3] R. A. Höpfel, J. Shah, P. A. Wolff, and A. C. Gossard, *Phys. Rev. Lett.* **56**, 2736 (1986).

[4] R. A. Höpfel and J. Shah, *Solid-State Electron.* **31**, 643 (1988).

- [5] T. J. Gramila, J. P. Eisenstein, A. H. MacDonald, L. N. Pfeiffer, and K. W. West, *Phys. Rev. Lett.* **66**, 1216 (1991).
- [6] P. M. Solomon, P. J. Price, D. J. Frank, and D. C. La Tulipe, *Phys. Rev. Lett.* **63**, 2508 (1989).
- [7] P. M. Solomon and B. Laikhtman, *Superlattices Microstruct.* **10**, 89 (1991).
- [8] W.-K. Tse, Ben Yu-Kuang Hu, and S. Das Sarma, *Phys. Rev. B* **76**, 081401(R) (2007).
- [9] S. Kim, I. Jo, J. Nah, Z. Yao, S. K. Banerjee, and E. Tutuc, *Phys. Rev. B* **83**, 161401(R) (2011).
- [10] S. Kim and E. Tutuc, *Solid State Commun.* **152**, 1283 (2012).
- [11] B. N. Narozhny, M. Titov, I. V. Gornyi, and P. M. Ostrovsky, *Phys. Rev. B* **85**, 195421 (2012).
- [12] J. C. W. Song, D. A. Abanin, and L. S. Levitov, *Nano Lett.* **13**, 3631 (2013).
- [13] A. Gamucci, D. Spirito, M. Carrega, B. Karmakar, A. Lombardo, M. Bruna, L. N. Pfeiffer, K. W. West, A. C. Ferrari, M. Polini, and V. Pellegrini, *Nat. Commun.* **5**, 5824 (2014).
- [14] J. I. A. Li, T. Taniguchi, K. Watanabe, J. Hone, A. Levchenko, and C. R. Dean, *Phys. Rev. Lett.* **117**, 046802 (2016).
- [15] A. H. Castro Neto, F. Guinea, N. M. R. Peres, K. S. Novoselov, and A. K. Geim, *Rev. Mod. Phys.* **81**, 109 (2009).
- [16] N. M. R. Peres, *Rev. Mod. Phys.* **82**, 2673 (2010).
- [17] S. Das Sarma, S. Adam, E. H. Hwang, and E. Rossi, *Rev. Mod. Phys.* **83**, 407 (2011).
- [18] M. F. Craciun, S. Russo, M. Yamamoto, and S. Tarucha, *Nano Today* **6**, 42 (2011).
- [19] E. H. Hwang, R. Sensarma, and S. Das Sarma, *Phys. Rev. B* **84**, 245441 (2011).
- [20] B. Amorim and N. M. R. Peres, *J. Phys.: Condens. Matter* **24**, 335602 (2012).
- [21] M. Carrega, T. Tudorovskiy, A. Principi, M. I. Katsnelson, and M. Polini, *New J. Phys.* **14**, 063033 (2012).
- [22] J. Lux and L. Fritz, *Phys. Rev. B* **86**, 165446 (2012).
- [23] M. Koebel, A. Rigacci, and P. Achard, *J. Sol-Gel Sci. Technol.* **63**, 315 (2012).
- [24] Y.-L. He and T. Xie, *Appl. Therm. Eng.* **81**, 28 (2015).
- [25] G. Tang, C. Bi, Y. Zhao, and W. Tao, *Energy* **90**, 701 (2015).
- [26] M. Fuji, C. Takai, H. Watanabe, and K. Fujimoto, *Adv. Powder Technol.* **26**, 857 (2015).
- [27] P. Gupta, B. Singh, A. K. Agrawal, and P. K. Maji, *Mater. Design* **158**, 224 (2018).
- [28] K. Flensberg and Ben Yu-Kuang Hu, *Phys. Rev. B* **52**, 14796 (1995).
- [29] S. M. Badalyan and F. M. Peeters, *Phys. Rev. B* **86**, 121405(R) (2012).
- [30] M. I. Katsnelson, *Phys. Rev. B* **84**, 041407(R) (2011).
- [31] A. Kamenev and Y. Oreg, *Phys. Rev. B* **52**, 7516 (1995).
- [32] A.-P. Jauho and H. Smith, *Phys. Rev. B* **47**, 4420 (1993).
- [33] W. Chen, A. V. Andreev, and A. Levchenko, *Phys. Rev. B* **91**, 245405 (2015).
- [34] F. Escudero and J. S. Ardenghi, *J. Phys.: Condens. Matter* **34**, 395602 (2022).
- [35] A. Levchenko and A. Kamenev, *Phys. Rev. Lett.* **100**, 026805 (2008).
- [36] M. Schütt, P. M. Ostrovsky, M. Titov, I. V. Gornyi, B. N. Narozhny, and A. D. Mirlin, *Phys. Rev. Lett.* **110**, 026601 (2013).
- [37] L. Hrubesh, L. Keene, and V. Latorre, *J. Mater. Res.* **8**, 1736 (1993).
- [38] L. W. Hrubesh, *J. Non-Cryst. Solids* **225**, 335 (1998).
- [39] S. Das Sarma, E. H. Hwang, and W.-K. Tse, *Phys. Rev. B* **75**, 121406(R) (2007).
- [40] G. Borghi, M. Polini, R. Asgari, and A. H. MacDonald, *Solid State Commun.* **149**, 1117 (2009).
- [41] M. C. Bønsager, K. Flensberg, Ben Yu-Kuang Hu, and A. H. MacDonald, *Phys. Rev. B* **57**, 7085 (1998).
- [42] B. Amorim, J. Schiefele, F. Sols, and F. Guinea, *Phys. Rev. B* **86**, 125448 (2012).
- [43] R. Fandan, J. Pedrós, F. Guinea, A. Boscá, and F. Calle, *Commun. Phys.* **2**, 158 (2019).
- [44] L. Zheng and A. H. MacDonald, *Phys. Rev. B* **48**, 8203 (1993).
- [45] J. Lux and L. Fritz, *Phys. Rev. B* **87**, 075423 (2013).
- [46] B. Scharf and A. Matos-Abiague, *Phys. Rev. B* **86**, 115425 (2012).
- [47] L. Zhu, L. Li, R. Tao, X. Fan, X. Wan, and C. Zeng, *Nano Lett.* **20**, 1396 (2020).